

<https://doi.org/10.1038/s43247-024-01295-w>

Hydrological drought forecasts using precipitation data depend on catchment properties and human activities

Check for updates

Samuel Jonson Sutanto , Wahdan Achmad Syaehuddin & Inge de Graaf

Hydrological Drought Early Warning Systems play a crucial role in effective drought planning and management, as the impacts of drought are more closely associated with hydrological droughts than meteorological ones. However, current systems primarily focus on meteorological drought forecasts due to the limited access to hydrological data. Here we assess the feasibility of forecasting drought in streamflow and groundwater by solely using precipitation data. The results demonstrate that meteorological drought forecasts derived from the Standardized Precipitation Index with 6-month accumulation periods and various lag times hold the potential to predict streamflow and groundwater droughts. This study also highlights the importance of catchment properties in hydrological drought predictions. Our findings present an opportunity for developing hydrological drought early warning system globally to reach the goal of the Sendai framework for disaster risk reduction by 2030 and support the initiative of early warnings for all.

Hydrological droughts, characterized by their creeping onset and prolonged duration, impose substantial human and economic losses, leading to a wide range of impacts^{1–3}. In response, many countries have established Drought Early Warning Systems (DEWSs) to reduce the adverse impacts of droughts. Yet, the current focus remains predominantly on meteorological drought forecast with short lead time^{4,5}. Many reported drought impacts, on the other hand, are more closely associated with hydrological droughts rather than meteorological ones, spanning critical areas such as public water supply, water-borne transportation, low hydropower energy production, and fisheries^{6–8}. This calls for the development of hydrological DEWSs capable of providing timely and accurate information on impending hydrological drought events several months in advance, which is an indispensable prerequisite for effective drought planning and management.

Despite the importance of hydrological drought forecasts, the development of hydrological DEWS has been hindered by various obstacles. One major challenge lies in the limited availability of hydrological data, both for observations and forecasts, especially when compared to the readily accessible meteorological data (e.g., precipitation), which is available at a global or country scale. Moreover, forecasting hydrological droughts require a state-of-the-art hydrological model that simulates relevant hydrology and atmospheric interactions⁵. Although hydrological models, such as LIS-FLOOD, the mesoscale hydrological model (mHM), the variable infiltration capacity (VIC) model and the Xinanjiang hydrological model (GXAJ) have

been implemented for monitoring and forecasting hydrological droughts in various regions^{5,9–12}, not all countries have the capacity to develop and operationally run the hydrological models. This limitation has resulted in hydrological DEWS not gaining important attention on political agendas in some European countries, particularly in the global south, where emphasis has been on the development of meteorological drought monitoring and DEWS⁴. It is important to distinguish between meteorological droughts and hydrological droughts^{13–16}. Meteorological drought may not always propagate into hydrological droughts, which means that meteorological drought cannot straightforwardly be used to predict drought in groundwater or river flow. On the contrary, hydrological droughts are consistently preceded by meteorological drought in the absence of anthropogenic influences¹⁷.

To bridge the gap in developing hydrological DEWS in regions with limited hydrological data and provide valuable insight into predicting hydrological droughts, we present a pioneering study in drought forecasting by utilizing seasonal precipitation forecasts. The aim was to assess the relation between meteorological and hydrological droughts, and under which assumptions meteorological droughts can be used to predict streamflow and groundwater droughts. Our study focuses on the identification of hydrometeorological droughts using the Standardized Precipitation Index (SPI)¹⁸ for meteorological drought, and the Standardized Streamflow Index (SSI-1)¹⁹ and the Standardized Groundwater Index (SGI-1)²⁰ for drought in streamflow and groundwater, respectively. We

Earth Systems and Global Change Group, Environmental Sciences Department, Wageningen University and Research, Droevendaalsesteeg 3a, 6708PB Wageningen, the Netherlands. e-mail: samuel.sutanto@wur.nl

focused our study in Europe, mainly motivated by the availability of high-resolution data that was used for the method and to evaluate the results. The streamflow and groundwater droughts were derived from the streamflow and groundwater data simulated using the LISFLOOD model. The LISFLOOD model simulates the full water cycle and is driven by observed and forecasted weather data to obtain the proxy observed data and forecasts, respectively^{21,22}. To assess the relationship between meteorological and hydrological droughts, a Pearson's correlation analysis and a time-lagged cross correlation were conducted, respectively^{23,24}. Lastly, we evaluated the performance of drought forecasts using the Brier Score (BS)²⁵ (Methods). Our results demonstrate that the SPI-6 with 1 month lag time emerged as the most effective predictor for forecasting hydrological droughts in numerous regions across Europe. The SPI-6 forecast performance remains comparable when evaluating hydrological droughts based on SSI-1 and SGI-1 forecasts.

Results

Correlation between meteorological and hydrological droughts

The standardized drought indices, such as SPI, SSI, and SGI quantify how the hydrometeorological data deviates from the long-term mean (see "Methods" section). To investigate the relation between meteorological and hydrological droughts in Europe, we calculated the SPI- x with different accumulation periods ($x = 1, 3, 6,$ and 12) based on observed data from 1991 to 2022. These SPI values were then correlated with proxy observed of SSI-1 and SGI-1 (Fig. 1). The results are visualized in boxplots showing the distribution of correlation values, including the 25th percentile, median, and 75th percentile, for all grid cells in Europe. The Pearson correlation values exhibit spatial variability and vary across different accumulation periods, ranging from -0.1 to 1 . Among different accumulation periods, SPI-6 generates the highest correlation with SSI-1, with a median correlation of 0.39 . SPI-12, however, yields a slightly lower correlation value of 0.35 compared to SPI-6 although the difference is not substantial. As expected, the shortest accumulation period, SPI-1, generates the lowest median correlation of 0.02 , which is also the case for correlation with SGI-1. The correlation between SPI-1 and SGI-1 has a median correlation value of 0.23 , which is the lowest compared to all accumulation periods. Notably, the correlation between SPI- x and SGI-1 is highest for SPI-6 (0.56), though the result is similar to SPI-12 (0.54).

Further analysis reveals that the correlation between SPI- x and the drought indices vary across different regions of Europe (Supplementary Fig. 1). In general, SPI-1 shows weak correlation with SSI-1 in most parts of

Europe, except for specific regions such as the Pyrenees, south of England, north of Sweden, and Turkiye (Supplementary Fig. 1a). Similarly, SPI-6, despite displaying the highest correlation overall, exhibits lower correlations in mountainous areas like the Pyrenees, north of Sweden, Norway, Alps, and north of Italy (Supplementary Fig. 1b), associated with the coarse model resolution in these regions²⁶. Rivers located in Portugal, France, Germany, south of England, and east Europe show a strong correlation with SPI-6. The correlation between SPI-1 and SGI-1 is higher compared to SSI-1 in many regions of Europe (Supplementary Fig. 1a, c). Nonetheless, the correlation increases when longer accumulation periods are used e.g., SPI-6 (Supplementary Fig. 1d). Notably, several regions in Europe demonstrate higher correlation values between SPI-6 and SGI-1 rather than with SSI-1.

To summarize the correlation patterns, we present the correlation values for each SPI- x and European regions in Table 1. The correlations between SPI- x and SSI-1 as well as SGI-1 are found to be significant ($p < 0.05$) for all indices except for SPI-1 (Supplementary Tables 1 and 2). Overall, the highest correlation between SPI- x and SSI-1 is observed in western Europe, followed by central, eastern, southern, and northern Europe. SPI-3 is best correlated with SSI-1 in western Europe (0.54) and southern Europe (0.37), while SPI-6 shows a good correlation in central (0.46), eastern (0.40), and northern Europe (0.33). However, the correlation between SPI-3 and SSI-1 in western and southern Europe is similar to that of SPI-6, with a maximum difference of 0.01 . Regarding groundwater drought, the highest correlations between SPI- x and SGI-1 are found for SPI-6 in western (0.68), northern (0.52), and southern Europe (0.53). For SPI-12, high correlations are observed with SGI-1 in central (0.58) and eastern Europe (0.57). The difference in correlation between SPI-6 and SPI-12 in indicating groundwater drought is relatively small. Lower correlation values between SPI- x and SSI-1 than between SPI- x and SGI-1 may be caused by the management of river discharge, especially in the north and south of Europe.

Given these findings, namely highest correlation and small difference with SPI-12, we simply select SPI-6 as the most suitable drought index for representing streamflow and groundwater droughts in Europe. Consequently, we focus on utilizing SPI-6 as our primary drought index for forecasting hydrological droughts, as it demonstrates the highest and most consistent correlations with the hydrological indices across various regions of Europe. For regional/small-scale studies, we recommend using the appropriate accumulation period that yields the highest correlation for that region. For instance, SPI-3 is better applied in south Europe to represent SSI-1.

Fig. 1 | Correlation between meteorological and hydrological droughts. Variability of correlation value between SPI- x and SSI-1 (blue color) and SPI- x and SGI-1 (yellow color). The lower box shows the 25 percentile, the middle line shows median, and the upper box shows the 75 percentile. The whiskers show the maximum and minimum correlations.

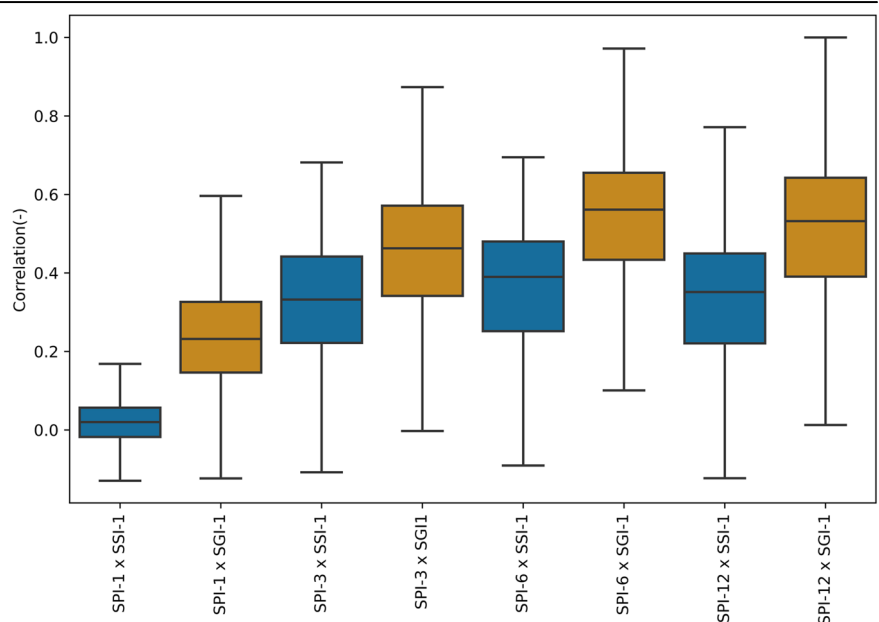


Table 1 | The mean correlation values of SPI-x and SSI-1, and SPI-x and SGI-1 for each European region

| Region in Europe | SSI-1 | | | | SGI-1 | | | |
|------------------|--------|--------------|--------------|--------|-------|-------|--------------|--------------|
| | SPI-1 | SPI-3 | SPI-6 | SPI-12 | SPI-1 | SPI-3 | SPI-6 | SPI-12 |
| WE | 0.007 | 0.539 | 0.531 | 0.434 | 0.354 | 0.600 | 0.678 | 0.631 |
| CE | -0.002 | 0.441 | 0.462 | 0.398 | 0.235 | 0.449 | 0.553 | 0.579 |
| EE | -0.016 | 0.321 | 0.401 | 0.397 | 0.186 | 0.428 | 0.555 | 0.565 |
| NE | 0.027 | 0.281 | 0.329 | 0.321 | 0.266 | 0.446 | 0.521 | 0.482 |
| SE | 0.028 | 0.372 | 0.371 | 0.326 | 0.277 | 0.470 | 0.531 | 0.489 |

Values in bold indicate the highest correlation for each region.

WE West Europe, CE Central Europe, EE East Europe, NE North Europe, SE South Europe.

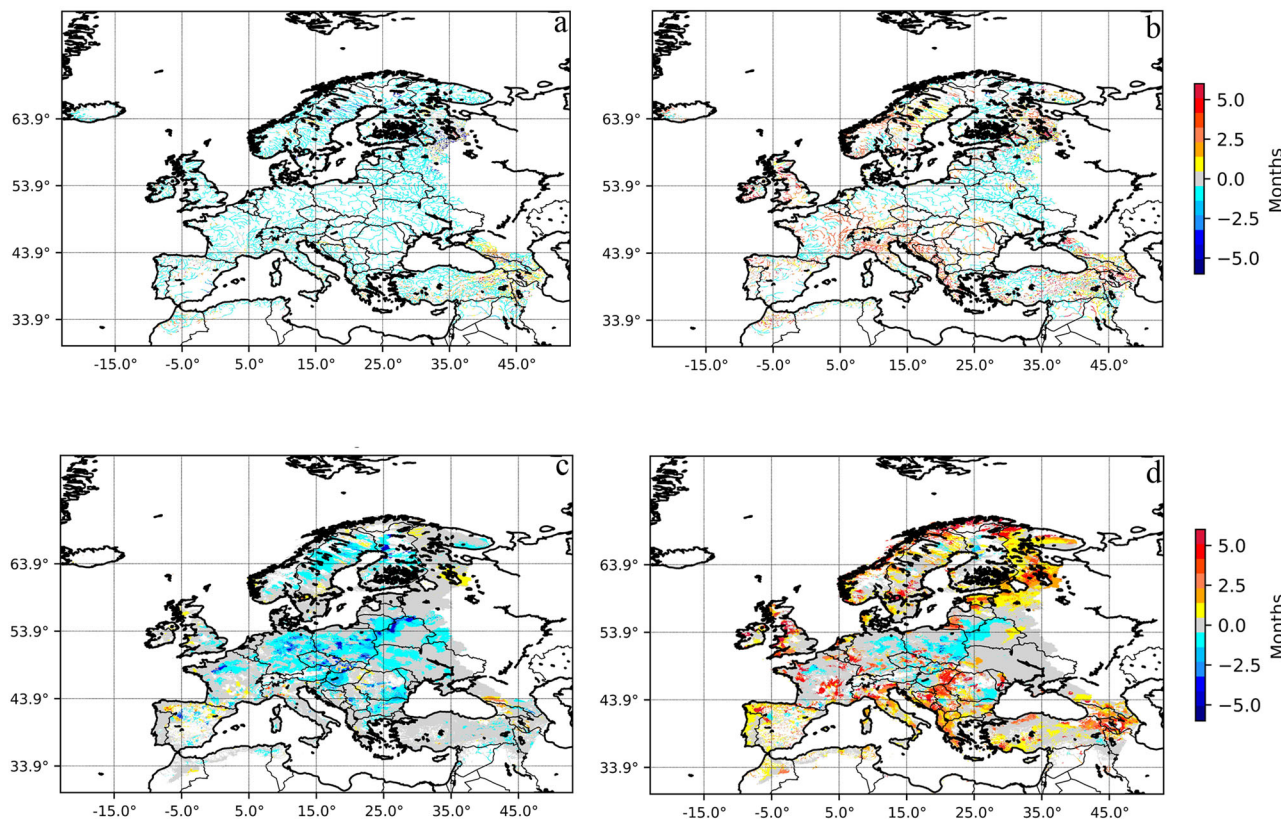


Fig. 2 | The lag time between meteorological and hydrological droughts for the Pan-European regions. a Lag time between SPI-6 and SSI-1. **b** Lag time between SPI-12 and SSI-1. **c** Lag time between SPI-6 and SGI-1. **d** Lag time between SPI-12 and SGI-1.

Meteorological drought propagation

A time-lagged cross correlation approach was employed to investigate the drought propagation process (lag time) between meteorological and hydrological droughts (Method)²⁴. The correlation analysis reveals both negative and positive lag times in the relationship between these two types of droughts (Fig. 2). Negative lag times indicate the time required for meteorological drought to propagate and manifest as hydrological droughts. On the other hand, positive lag times imply that hydrological droughts precede meteorological drought events, which is not a common case. Several factors can contribute to positive lag times. For instance, multiple hydrological drought events may take place after short periods of rain, followed by subsequent meteorological drought events. Additionally, in the case of correlations between SPI-12 and SGI-1, multi-year drought events may also contribute to positive lag times. For this study, we did not apply the pooling approach to minimize minor drought events^{14,27}. Thus, we focused on the negative lag times, which provide a clear signal of meteorological drought propagating to hydrological droughts. Consequently, positive lag times were

neglected in our methodology, and only negative lag times were considered for analysis.

In general, the correlation analysis between SPI-6 and SSI-1 shows a predominant negative lag time of 1 month in most European river branches (light blue color, Fig. 2a). However, a few river branches exhibit positive lag times of 1 till 5 months (yellow to reddish colors). For the correlation between SPI-12 and SSI-1, positive lag times of up to 5 months are observed in certain rivers located in the UK, northern Italy, and from Slovenia to Greece (Fig. 2b). Similarly, negative correlations between SPI-6 and SGI-1 are also found in many regions, particularly in western and central Europe (Fig. 2c). Correlations of SPI-12 and SGI-1 yield positive lead times in numerous European regions, notably in Spain, Albania, Macedonia, and Greece (Fig. 2d). On average, the lag time between the SPI-6 and the occurrence of hydrological drought is close to 0 and 2 months, depending on the region of interest and drought indices. SPI-6 with a lag time of 1 month generally exhibits a stronger correlation with SSI, while SPI-6 with lag times of 0–2 months can effectively represent groundwater drought. Unlike the

SPI-6 that was chosen to represent the whole of Europe, we applied various negative lag times as depicted in Fig. 2a, c to the forecasted SPI-6 and evaluated the forecast performance compared to SSI-1 and SGI-1 accordingly.

Performance of meteorological drought to predict hydrological droughts

To assess the potential of meteorological drought (SPI-6) in forecasting hydrological droughts (SSI-1 from 1991 to 2022 and SGI-1 from 2002 to 2016 as benchmarks), we evaluate the performance of median SPI-6 forecasts (out of 25 and 51 ensemble members, see “Methods” section) across Europe (Fig. 3). Different lag times (Fig. 2) were applied to SPI-6 forecasts that were clipped by river grid cells to match with the SSI-1. In western European regions, such as the southwestern of UK, France, the Netherlands, and Germany, the forecast performance for streamflow drought with a lead time of 1 month (LT = 1) is the highest (average BS = 0.195) when using SPI-6 forecasts with different lag times (Fig. 3a). Conversely, forecast performance is lower in the north of Europe (average BS = 0.252) and in the south of Europe (average BS = 0.250), with the exception for Portugal. Regions characterized by mountainous terrain, such as the Alps and Pyrenees, as well as areas influenced by snow and glacier (Scandinavia and Iceland) yield the lowest forecast performance.

Figure 3b depicts the performance of SPI-6 with various lag times to forecast groundwater drought (SGI-1). Similar to the results for SSI-1, the highest forecast performance for groundwater drought is observed in the southwest of the UK, the Netherlands, France, Germany, and Portugal, with average BS < 0.2. The presence of aquifers in the southwest of the UK and France may explain the high forecast performance due to the influence of groundwater on streamflow^{15,28}. SPI-6 forecasts show low performance in central, northern, and southern Europe. In the northern regions, particularly in Scandinavia, forecast performance may be influenced by the mismatch in snowmelt and accumulation timing, associated with biases in temperature prediction²⁹. Additionally, this area is predominantly characterized by glaciers rather than groundwater as it is situated in locally non-aquiferous rock formations³⁰. In eastern Europe, where the forecast performance for streamflow drought is relatively low (BS = 0.2–0.3), SPI-6 yields higher forecast performance for groundwater drought (BS < 0.2). This region is characterized by moderately to highly productive porous aquifers^{30,31}, which implies relatively fast groundwater recharge. In addition, the rivers in this region are not strongly contributed by groundwater but by precipitation, resulting in a low to moderate baseflow index (BFI²⁸).

Figure 4 presents the summary of SPI-6 drought forecast performance in predicting hydrological droughts at the scale of Europe, considering different seasons, lead times, and regions. The results show that SPI-6 performs best in autumn (BS = 0.229 and 0.210) and winter (BS = 0.247 and 0.212) for both SSI-1 and SGI-1 (Fig. 4a, d, respectively), which may be

attributed to more accurate precipitation predictions for these seasons by the SEAS5, particularly in response to the North Atlantic Oscillation (NAO)^{16,32,33}. Regions, such as the south of the United Kingdom, the Netherlands, Belgium, Germany, and north of France show high hydrological drought prediction performance in these seasons, with BS < 0.2 (Supplementary Figs. 3 and 4). The lowest performance is observed in spring for SSI-1 (BS = 0.258) and in summer for SGI-1 (BS = 0.227), which can be explained by the discrepancies in the predictions of intense summer precipitation events, evapotranspiration, and snowmelt in spring^{29,34,35}. In Spring, streamflow drought predictions are more accurate in specific regions in western Europe, such as south of the United Kingdom, the Netherlands, Belgium, Portugal, and west France, but performance improves in summer for Germany, Poland, and north of France (Supplementary Fig. 3b, c). During the summer season, the SGI-1 displays the lowest performance in Spain, south of France, and in some southeastern European countries (Supplementary Fig. 4c). As expected, the forecast performance decreases as the lead times become longer (Fig. 4b, e). Regarding the regional variations in forecast performance, streamflow drought prediction using SPI-6 exhibits the highest performance in western Europe (BS = 0.195), followed by central Europe (BS = 0.220), eastern Europe (BS = 0.228), south Europe (BS = 0.250), and northern Europe (BS = 0.252) (Fig. 4c). Similarly, SPI-6 demonstrates the highest performance in predicting groundwater drought in western Europe (BS = 0.184) and the lowest performance in southern Europe (BS = 0.224, Fig. 4).

Comparison with hydrological drought forecasts

In previous section, we evaluated the performance of SPI-6 to predict droughts in streamflow and groundwater derived from observed SSI-1 (SSI-1_{SPI-6}) and SGI-1 (SGI-1_{SPI-6}), respectively (Method). Here, we compare the performance of SPI-6 in predicting hydrological droughts (SSI-1_{SPI-6} for streamflow and SGI-1_{SPI-6} for groundwater) against the forecasted SSI-1 and SGI-1 derived from the forecasted streamflow and groundwater, respectively. The results indicate that, for most seasons and lead times, SSI-1_{SPI-6} predicts lower performance than SSI-1, with the exception of winter for LT = 1 (Fig. 5a). Overall, the annual average of SSI-1 yields slightly higher performance (BS = 0.250, LT=1) in predicting streamflow drought compared to SSI-1_{SPI-6} (BS = 0.257, LT = 1), although the difference is relatively small. This outcome is expected since precipitation is not the sole variable influencing river discharge. As the lead times increase, the difference in forecast performance between SSI-1_{SPI-6} and SSI-1 becomes larger with a maximum difference of 0.037 observed in summer (LT = 4).

The comparison between SGI-1_{SPI-6} and SGI-1 indicates that the forecast performance of groundwater drought identified using both indicators is higher than the streamflow drought forecasts, with a maximum BS of 0.241 for LT = 1 (Fig. 5b vs 5a). When SPI-6 is used to identify groundwater drought (SGI-1_{SPI-6}), the forecast performance is slightly

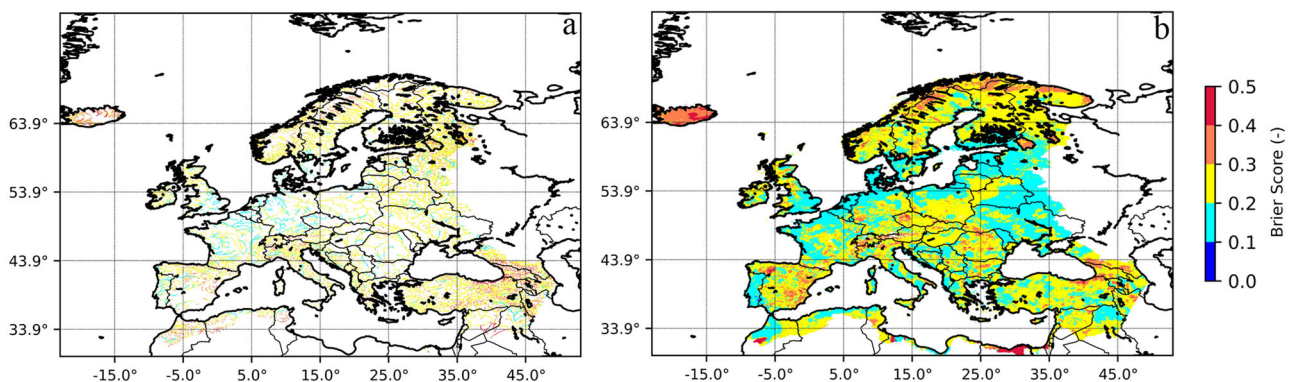


Fig. 3 | The performance of SPI-6 to identify hydrological droughts. **a** The performance of median SPI-6 to identify streamflow drought (SSI-1) with a lead time of 1-month. **b** The performance of median SPI-6 to identify groundwater drought

(SGI-1) with a lead time of 1-month. Bluish colors indicate high forecast performance and vice versa for reddish colors.

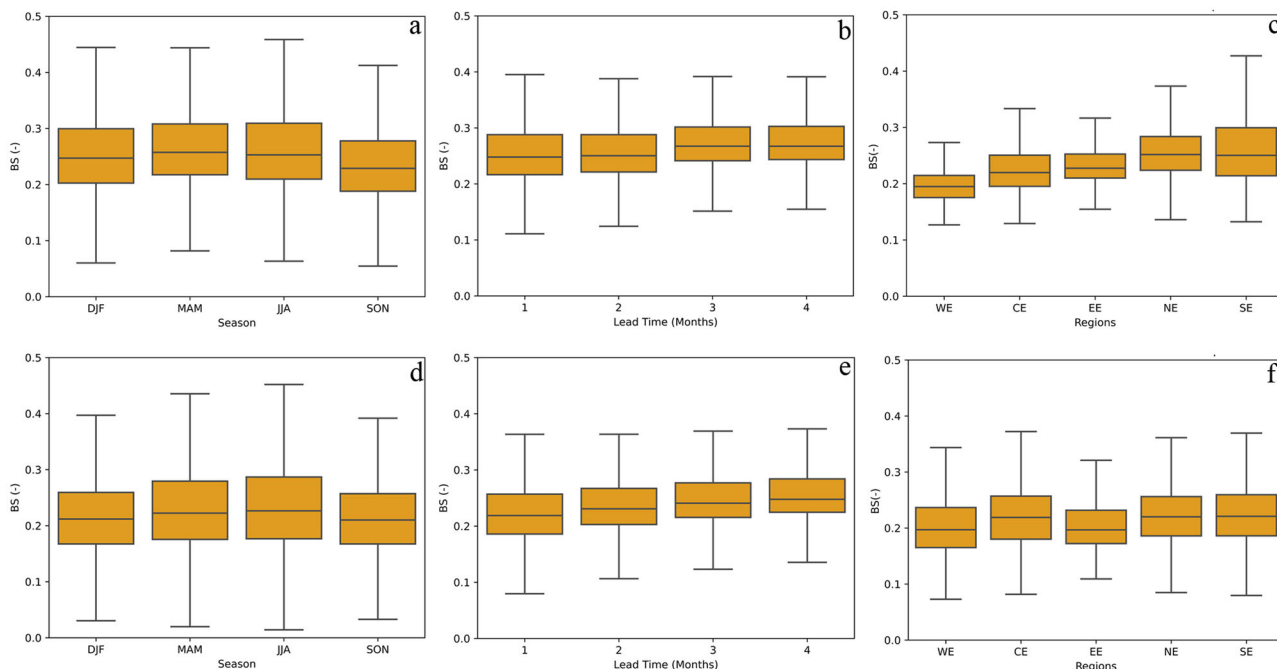


Fig. 4 | Box plot showing the performance of SPI-6 to identify hydrological droughts. **a** The performance of SPI-6 to identify streamflow drought (SSI-1_{SPI-6}) for each season. **b** The performance of SPI-6 to identify streamflow drought (SSI-1_{SPI-6}) for different lead times. **c** The performance of SPI-6 to identify streamflow drought (SSI-1_{SPI-6}) for each European region. **d** The performance of SPI-6 to

identify groundwater drought (SGI-1_{SPI-6}) for each season. **e** The performance of SPI-6 to identify groundwater drought (SGI-1_{SPI-6}) for different lead times. **f** The performance of SPI-6 to identify groundwater drought (SGI-1_{SPI-6}) for each European region. WE West Europe, CE Central Europe, EE East Europe, NE North Europe, SE South Europe.

lower than using SGI-1 (Fig. 5b). The difference in performance between SGI-1_{SPI-6} and SGI-1, however, remains relatively constant up to LT = 3 and starts to deviate at LT = 4. The annual average of SGI-1 yields BS of 0.227 for LT = 1, which is slightly higher than SGI-1_{SPI-6} (BS = 0.229). Unlike SSI-1, where there is a slightly larger performance gap between SSI-1 and SSI-1_{SPI-6} in almost all seasons and lead times, SGI-1_{SPI-6} exhibits smaller gaps in the forecast performance compared to SGI-1. The lowest SGI-1_{SPI-6} performance is observed only in summer with BS values of 0.241 for LT = 1 and 0.285 for LT = 4.

Regionally, the forecasting of streamflow drought using SPI-6 (SSI-1_{SPI-6}) demonstrates added value in CE and SE, exhibiting slightly higher forecast performance compared to SSI-1 (Fig. 5c, detail in Supplementary Table 3). SSI-1_{SPI-6} yields BS scores of 0.237 and 0.255, while SSI-1 generates BS scores of 0.255 and 0.266 in CE and SE, respectively. On the other hand, SGI-1_{SPI-6} shows higher performance in WE and CE, with BS values of 0.221 and 0.235, respectively, compared to SGI-1 (BS = 0.228 for WE and 0.261 for CE) (Fig. 5d). Many areas in WE and CE are classified as having fast-declining groundwater level, which strongly influences the performance of streamflow and groundwater drought forecasts²⁸. In addition, the lower performance of the LISFLOOD models in simulating streamflow in SE may contribute to reduced performance of SSI-1³⁶. In other regions, SSI-1 and SGI-1 consistently outperform drought forecasts using SPI-6, with generally small differences, up to Δ BS = ~0.01, except in NE for both streamflow and groundwater droughts. Overall, the forecasts based on SSI-1 and SGI-1 demonstrate better forecasting performance than using SPI-6.

Discussion

The correlation analysis between SPI with different accumulation periods and hydrological droughts (SSI-1 and SGI-1) across Europe reveals spatial variability in the relationships (Supplementary Figs. 1 and 2 and Table 1). This indicates that there is no universal SPI-x that can effectively represent the hydrological droughts for the entire region. Instead, the correlation

patterns are influenced by catchment properties in different areas. For example, in England and Wales, SPI with shorter accumulation periods correlates well with SGI-1 in the north, while SPI with longer accumulation periods correlates better in the south (Supplementary Fig. 1c, d), where major aquifers are located. This means that this region is characterized by groundwater-fed rivers on permeable aquifer¹⁵. The influence of catchment properties is further demonstrated in southern Spain, where SPI-6 shows a high correlation with hydrological drought possibly due to the presence of limestone headwaters³⁷, while in the Pyrenees, SPI-1 exhibits strong correlation with SSI-1 likely because of its fast response catchment³⁸. Previous research in Europe has also suggested that SPI has an increased correlation with SGI-1 until 6- and 12-month accumulation periods (SPI-6 and SPI-12), depending on the depth of the groundwater level^{39,40}. Kumar et al.³⁹ and Haas and Birk⁴⁰ studies concluded that SGI is highly correlated with SPI-6 and SPI-12 in shallow and deep wells, respectively. In this study, the LISFLOOD groundwater data is obtained from the top layer or shallow groundwater systems, which correspond better with SPI-6. These findings emphasize that catchment specific properties are driving the number of accumulation months required to indicate hydrological droughts.

In addition to catchment properties, anthropogenic activities can strongly influence the relationship between SPI-x and hydrological droughts. Our results reveal that the correlation between SPI-x and SSI-1 is lower compared to the correlation between SPI-x and SGI-1, particularly in the NE and SE regions (Fig. 1 and Table 1). The development of water infrastructures, such as reservoirs and dams, is conjectured as the main reason for the lower correlation. This impact is pronounced in northern and southern Europe, where river regimes have been altered substantially with the development of infrastructure, mainly for hydropower, water supply, and irrigation^{37,41}. For example, the Guadiana catchment in Spain alone hosts 39 reservoirs⁴². Furthermore, the management of river discharge across Europe, especially in the northeast and southeast, exerts a substantial influence on the performance of streamflow forecasts^{43,44} and thus translates into lower performance of streamflow drought forecast²⁸.

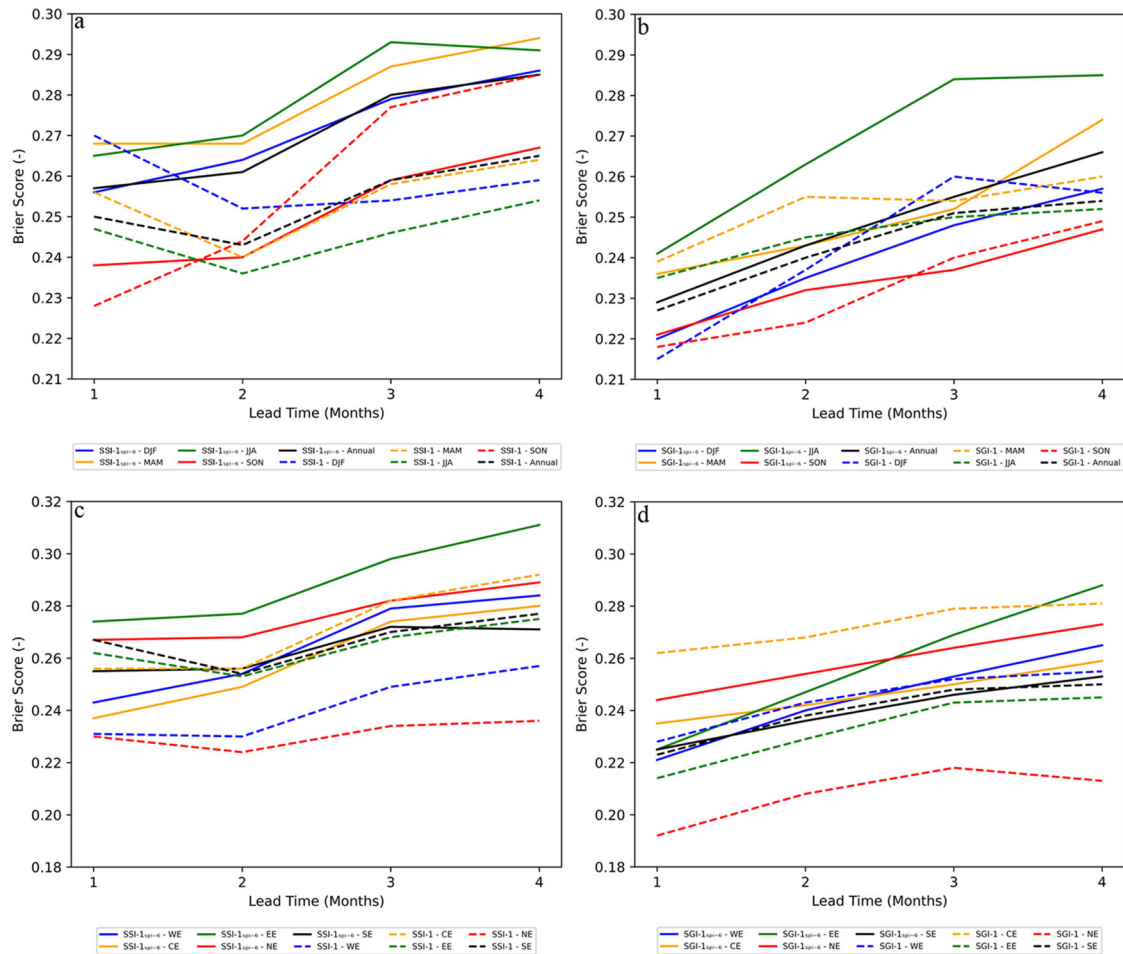


Fig. 5 | Comparison of Brier Score values among diverse drought forecasts.

a Comparison of Brier Score (BS) values between SSI-1 forecasted using SPI-6 (SSI-1_{SPI-6}) and SSI-1 forecast for different seasons. **b** Comparison of BS values between SGI-1 forecasted using SPI-6 (SGI-1_{SPI-6}) and SGI-1 forecast for

different seasons. **c** Comparison of BS values between SSI-1 forecasted using SPI-6 (SSI-1_{SPI-6}) and SSI-1 forecast for each region. **d** Comparison of BS values between SGI-1 forecasted using SPI-6 (SGI-1_{SPI-6}) and SGI-1 forecast for each region.

The longer accumulation periods for SPI to represent SSI-1 and SGI-1 are expected since SPI- x with $x > 1$ month is suggested to capture both agricultural and hydrological droughts^{2,45}. Specifically, SPI-3 is considered more suitable to detect agricultural drought, while SPI-6 and SPI-12 are deemed better suited to represent hydrological droughts. A prior study in Germany also indicated a relationship between drought indicators with different accumulation period and their corresponding impacts⁴⁶. A 3-month accumulation period was identified as the optimal predictor for agricultural impacts, while longer accumulation periods were preferred as predictors for hydrological impacts such as those affecting energy and industry. The use of SSI or SGI with longer accumulation periods (e.g., 3 and 6 months) may better represent long hydrological droughts (e.g., multi-year drought). The applicability, however, remains a subject of debate, given that streamflow and groundwater already comprise the accumulation and delay of the meteorological signal due to catchment properties^{20,47,48}. In this study, therefore, we opted to exclusively applied SSI and SGI with 1-month accumulation period.

Similar to SPI drought aggregation, the lag time required for meteorological drought to transform into hydrological droughts varies in each region, especially for SGI-1. In many European regions, the lag time between SPI-6 and SGI-1 ranges from 0 to 1 month, while in some areas, longer lag times of > 2 months are observed. This variation in lag time underscores the influence of catchment properties in drought propagation, where hydrological drought will form quickly in the fast-responding catchment, and vice versa for slow-responding catchment^{17,49}. A study in 14 sites across UK also

shows that chalk (fractured) aquifers have longer lag times of 1 to 2 months compared to limestone (fractured) aquifers, which has no lag time²⁰. Moreover, applying appropriate lag time to SPI-6 forecasts improves forecast performance from BS = 0.267 to BS = 0.257 for SSI-1_{SPI-6} and from BS = 0.230 to BS = 0.229 for SGI-1_{SPI-6} (Supplementary Tables 4 and 5, respectively). As a result, the SPI-6 forecasts could better mimic the SSI-1 and SGI-1 performance when different lag times were applied.

Our results clearly highlight the importance of catchment response in hydrological drought predictions. We found that the performance of drought forecasts using both SGI-1_{SPI-6} and SGI-1 is higher compared to SSI-1_{SPI-6} and SSI-1²⁸. Groundwater as the slowest responding variable to precipitation, depending on the aquifer properties, exhibits higher predictability than streamflow. This finding is consistent with previous studies on seasonal streamflow forecasting, which also conclude that streamflow can be better forecasted for rivers located in slower-responding catchments e.g., higher baseflow index (BFI) and high groundwater storage^{28,43,44,50}. It is important to note that despite SPI-6 produces lower performance than individual drought indices, i.e., SSI-1 and SGI-1, the discrepancy in forecast performance between SPI-6 and the specific hydrological drought indices is relatively small. Despite the lower performance, SPI-6 with applied lag times still provides valuable information and reasonable forecast accuracy for hydrological droughts.

An alternative method for forecasting hydrological drought involves the use of Ensemble Streamflow Prediction (ESP), derived from long-term observational data. However, some previous studies have indicated that

drought forecasts derived from the ECMWF dynamical forecasts, as employed in this study, exhibit considerably higher skill than ESP for meteorological drought and slightly better skill for hydrological drought^{16,33,51}. Thus, the ESP can be another potential source of hydrological forecasts if dynamical precipitation forecast is not available, which is not the case across Europe.

In our study, we utilized the ERA5 and SEAS5 datasets to identify historical and forecasted meteorological droughts (SPI), respectively, and the LISFLOOD model driven by these datasets for simulating the streamflow and groundwater. The simulated (proxy observed) and forecasted hydrological variables were then translated into droughts in streamflow and groundwater using the standardized drought indices, SSI and SGI. Both ERA5 and SEAS5 employ similar ECMWF Integrated Forecasting System (IFS) Cy41r2 and Cy43r1 to generate the proxy observed and forecast data, respectively^{52,53}. Using similar systems/models is expected to result in lower bias compared to using other datasets⁵⁴. The use of ground observations and remote sensing data, such as satellite altimetry and the Global Runoff Data Centre (GRDC) for streamflow^{55,56} as well as Gravity Recovery and Climate Experiment (GRACE)⁵⁷ may offer alternatives to proxy observed data for hydrological drought monitoring. For hydrological drought forecasting, however, a hydrological model forced with meteorological forecast data is a prerequisite. Thus, we suggest bias-correcting the forecast data and using the same forcing data (e.g., remote sensing) to initialize the hydrological model if alternative observational datasets are preferred.

This study represents a pioneering effort in forecasting hydrological droughts by leveraging meteorological drought forecasts with consideration of different accumulation periods and lag times. The successful application of meteorological drought forecasts for predicting hydrological droughts with comparable performance to direct hydrological drought predictions underscores the potential of this approach as a valuable alternative when hydrological forecast data is unavailable. This is often the case in many countries, particularly emerging ones. However, it should be noted that this approach is best applied in the area that is less influenced by anthropogenic activities. Anthropogenic factors, such as the management of river discharge and aquifers, can reduce the performance of hydrological forecasts, subsequently impacting hydrological drought predictions. Given the widespread availability of precipitation forecasts through meteorological agencies, the methods employed in this study hold broad applicability on a global scale. The findings, therefore, have important theoretical implications, particularly in developing hydrological DEWS. This progress aligns with the objective of the Sendai framework for disaster risk reduction and provides valuable support to the United Nations' Early Warnings for All initiative.

Methods

Data

Two types of datasets were used for both meteorological and hydrological data. For meteorological data, the first dataset comprised precipitation observations obtained from the European Centre Medium-range Weather Forecast (ECMWF) reanalysis product version 5 (ERA5)⁵³. Although ERA5 is not a ground observation product, ERA5 sometimes is treated as a proxy observed dataset due to the assimilation of a vast amount of observation data, totaling around 94.6 billion observations^{58,59}. ERA5 data was downloaded from January 1991 to December 2022. The second dataset consisted of the ECMWF seasonal forecast version 5 (SEAS5) with a lead time of 7 months⁶⁰. The precipitation reforecast data from 1993 to 2016 with 25 ensemble members and forecast data from 2017–2022 with 51 ensemble members were used. Both ERA5 and SEAS5 datasets were downscaled using the bilinear interpolation method from their original grid sizes to 5×5 km to match the LISFLOOD model outputs. Observational datasets, such as ground observations and remote sensing, were not used in this study. In fact, ERA5 consists of these observations and modeled data to fill in the data gap. Moreover, combining datasets other than ERA5 with SEAS5 would introduce high uncertainties due to differences in the nature of models and forcing data for the forecasts. The use of ERA5 as proxy observed and SEAS5 as seasonal forecasts aims to minimize these uncertainties. Both SEAS5 and

ERA5 rely on the ECMWF Integrated Forecasting System (IFS) with different configurations.

The hydrological data employed in the study were obtained from the European Flood Awareness System (EFAS)^{61,62}. EFAS utilizes the LISFLOOD hydrological model to simulate hydrological variables across Europe at a spatial resolution of 5×5 km. Please see Van der Knijff et al.²² and Burek et al.⁶³ for the model description. The observed hydrological data was derived from the LISFLOOD model run with gridded meteorological data (>5000 ground observations)⁶¹, known as simulation forced with observed (SFO) or proxy observed data. The (re)forecasts, on the other hand, were obtained from the LISFLOOD model forced with the SEAS5 meteorological data. The seasonal forecasts are available as daily data for each month from day 1 to day 215, aggregated into monthly data (7-month lead time). In this study, EFAS-observed hydrological data from 1991 to 2022 was used. Reforecast hydrological data from 1991 to 2020 and forecast data from 2021 to 2022 with 51 ensemble members were utilized. Please note, that only LISFLOOD observed groundwater data at the top layer from 1991 to 2018 and reforecast groundwater from 2002 to 2016 were used due to data availability constraints, which limits our study. These data are not available in the Copernicus Data Store (CDS) and were collected for the ANYWHERE project³. Despite these limitations, we believe that adding more data will not alter our conclusion that SGI can be better predicted than SSI. The LISFLOOD model incorporates water abstraction modules e.g., abstraction for irrigation, the livestock, energy production and cooling, and manufacturing industry, as well as 1454 reservoirs across Europe³⁶. The LISFLOOD model is commonly used for drought simulations implemented in the European DEWS^{5,64}. The use of proxy observed data is commonly accepted in forecast evaluation studies^{33,51,54,65}. A previous study analyzed the use of LISFLOOD proxy observed data compared to gauging data and found that the drought forecast performance is lower when gauging data is used as a benchmark⁶⁶. This study, however, did not bias-correct the forecast data, even though they used the gauging data to recalculate drought parameter distributions and threshold levels.

Model performance

The LISFLOOD model used in this study underwent calibration using a comprehensive set of observed streamflow time series from over 700 calibration stations across Europe³⁶. The performance evaluation based on the Kling-Gupta Efficiency (KGE) revealed that 42% of all calibration stations score a KGE higher than 0.75, 33% of all stations score a KGE between 0.5 and 0.75, and 25% of all stations score a KGE below 0.5, which indicates the good model's performance. The LISFLOOD model has also been used in various drought studies^{5,28,67–69}. Their studies show that the model performs rather well for drought identification, forecasting, and projection.

Standardized drought indices

Meteorological and hydrological droughts based on precipitation, streamflow, and groundwater data were identified using the Standardized Precipitation Index (SPI- x)¹⁸ with different accumulation periods of $x = 1, 3, 6, 12$, the Standardized Streamflow Index (SSI-1)¹⁹, and the Standardized Groundwater Index (SGI-1)²⁰, respectively. We only employed 1-month accumulation period for SSI and SGI because these indices already encompassed the accumulation and delay of the meteorological signal caused by e.g., groundwater flow and catchment. Therefore, hydrological drought indices, such as SSI and SGI are commonly calculated using only 1 month accumulation period^{20,47,70}. The standardized drought indices provide a measure of dryness by quantifying the deviation from the long-term mean, i.e. number of standard deviations. The drought indices were calculated by fitting a probabilistic distribution on monthly hydrometeorological data. To compute the standardized indices, the monthly hydrometeorological data was transformed into 12 distributions, corresponding to each index, accumulation period, and month of the year. Previous studies indicated that one single distribution does not fit all streamflow regimes in Europe and the distribution may vary each month^{48,70}. Therefore, there is no universal distribution for the whole

Europe that can be applied. For simplicity, we employed gamma distribution for all drought indices. Moreover, the gamma distribution has quite a flexible shape parameter, which is suitable for a wide range of drought application in EU^{69,71}. This distribution is described by two parameters: α (the shape parameter) and β (the inverse scale parameter). These distribution parameters then were used to calculate observed and (re)forecast drought events (for further details, refer to Sutanto et al.⁵). We define a drought event when the drought index values fall below -0.5, otherwise no drought^{51,66}.

Correlation and lag time analysis

The objective of the correlation analysis between SPI-x and SSI-1, as well as SGI-1, is to determine the most suitable accumulation time for SPI-x that can be used to forecast hydrological droughts. In this study, Pearson's correlation coefficient was employed to assess the relationship between meteorological and hydrological droughts^{2,23}. The correlation coefficient ranges from -1 to 1, with -1 representing a perfect linear negative correlation, 0 representing no correlation, and 1 representing a perfect linear positive correlation. A positive correlation suggests that as one variable increases, so does the other, whereas a negative correlation indicates that as one variable increases, the other decreases. The strength of the correlation is determined by how close the correlation coefficient is to 1 or -1.

The lag time was determined based on the correlation values of drought indices from 1991 to 2022. We applied the time-lagged cross correlation approach²⁴. This method maintains the time series of dependent variable (i.e., SSI and SGI) and generates both lags and leads of the second variable (SPI) throughout the time period. The time-lagged cross correlation approach results in a time series illustrating the relationship between time lags and correlation coefficients. We selected the lag time based on the highest correlation coefficient. A positive lag time indicates that hydrological drought occurs before meteorological drought, which was neglected in our study. A negative lag time indicates that hydrological drought occurs after meteorological drought.

Forecasting performance

The Brier Score (BS) is used in this study to evaluate the performance of the drought forecasts²⁵. This method involves comparing the predicted probability of a drought event (p) to the observed outcome (o). A lower BS indicates a more accurate forecast, with BS = 0 indicates perfect prediction. BS < 0.25 indicates forecasts that have higher performance than climatological forecast with $p = 0.5$ ⁷². BS of the forecast is then calculated by summing the squared difference between the predicted probability of an event (p ; range from 0 to 1) and the observed (o), divided by the total length of the data (N). It is important to distinguish that the BS describes forecast performance, and it should not be confused with the Brier Skill Score (BSS), which quantifies the skill of the forecast.

Data availability

The historical and seasonal (re)forecasts from EFAS are accessible through the Copernicus Data Store (CDS), which are freely available (<https://cds.climate.copernicus.eu/cdsapp#!/dataset/efas-seasonal-forecast?tab=form> and <https://cds.climate.copernicus.eu/cdsapp#!/dataset/efas-seasonal?tab=overview>). ERA5 and SEAS5 data are also accessible through the Copernicus Data Store (CDS) (<https://cds.climate.copernicus.eu/cdsapp#!/dataset/reanalysis-era5-single-levels?tab=overview> and <https://cds.climate.copernicus.eu/cdsapp#!/dataset/seasonal-original-single-levelst?tab=form>). Other data generated and/or analyzed during this study are available online in the 4TU Centre for Research Data using the link <https://doi.org/10.4121/302cd0fd-59da-46e8-ac82-f98fad865751> (Sutanto and Syaehuddin, 2024).

Code availability

All codes used to conduct the analysis presented in this paper are available online via <https://doi.org/10.4121/302cd0fd-59da-46e8-ac82-f98fad865751>.

Received: 3 October 2023; Accepted: 28 February 2024;

Published online: 07 March 2024

References

- Georgi, B. et al. Urban adaptation to climate change in Europe: Challenges and opportunities for cities together with supportive national and European policies. *Tech. Rep. EEA* <http://www.eea.europa.eu/publications/urban-adaptation-to-climate-change> (2012).
- Van Loon, A. F. & Laaha, G. Hydrological drought severity explained by climate and catchment characteristics. *J. Hydrol.* **526**, 3–14 (2015).
- Stahl, K. et al. Impacts of European drought events: insights from an international database of text-based reports. *Nat. Hazards Earth Syst. Sci.* **16**, 801–819 (2016).
- Pozzi, W. et al. Toward global drought early warning capability. *B. Am. Meteorol. Soc.* **94**, 776–785 (2013).
- Sutanto, S. J., Van Lanen, H. A. J., Wetterhall, F. & Llort, X. Potential of pan-European seasonal hydro-meteorological drought forecasts obtained from a multi-hazard early warning system. *B. Am. Meteorol. Soc.* **101**, 368–393 (2020).
- de Brito, M. M. Compound and cascading drought impacts do not happen by chance: A proposal to quantify their relationships. *Sci. Total Environ.* **778**, 146236 (2021).
- Turner, S. et al. The 2018/2019 drought in the UK: a hydrological appraisal. *Weather* **76**, 248–253 (2021).
- Blauhut, V. et al. Lesson from the 2018–2019 European droughts: a collective need for unifying drought risk management. *Nat. Hazards Earth Syst. Sci.* **22**, 2201–2217 (2022).
- Sheffield, J. et al. A drought monitoring and forecasting system for sub-Saharan African water resources and food security. *Bull. Amer. Meteor. Soc.* **95**, 861–882 (2014).
- Zink, M. et al. The German drought monitor. *Environ. Res. Lett.* **1**, 074002 (2016).
- Yuan, X., Zhang, M., Wang, L. & Zhou, T. Understanding and seasonal forecasting of hydrological drought in the Anthropocene. *Hydrol. Earth Syst. Sci.* **21**, 5477–5492 (2017).
- Lai, C. et al. Monitoring hydrological drought using long-term satellite-based precipitation data. *Sci. Total Environ.* **649**, 1198–1208 (2019).
- Mishra, A. K. & Singh, V. P. A review of drought concepts. *J. Hydrol.* **391**, 202–216 (2010).
- Van Loon, A. F. & Van Lanen, H. A. J. A process-based typology of hydrological drought. *Hydrol. Earth Syst. Sci.* **16**, 1915–1946 (2012).
- Barker, L. J., Hannaford, J., Chiverton, A. & Svensson, C. From meteorological to hydrological drought using standardized indicators. *Hydrol. Earth Syst. Sci.* **20**, 2483–2505 (2016).
- Sutanto, S. J., Wetterhall, F. & Van Lanen, H. A. J. Hydrological drought forecasts outperform meteorological drought forecasts. *Environ. Res. Lett.* **15**, 084010 (2020).
- Van Loon, A. F., Van Huijgevoort, M. H. J. & Van Lanen, H. A. J. Evaluation of drought propagation in an ensemble mean of large-scale hydrological models. *Hydrol. Earth Syst. Sci.* **16**, 4057–4078 (2012).
- McKee, T. B., Doesken, N. J. & Kleist, J. The relationship of drought frequency and duration to time scale. In *Proc. of 8th Conference on Applied Climatology*, 179–184 (American Meteorological Society, 1993).
- Nalbantis, I. & Tsakiris, G. Assessment of hydrological drought revisited. *Water Resour. Manag.* **23**, 881–897 (2009).
- Bloomfield, J. P. & Marchant, B. P. Analysis of groundwater drought building on the standardized precipitation index approach. *Hydrol. Earth Syst. Sci.* **17**, 4769–4787 (2013).
- Thielen, J., Bartholmes, J., Ramos, M.-H. & de Roo, A. The European flood alert system-part 1: concept and development. *Hydrol. Earth Syst. Sci.* **13**, 125–140 (2009).

22. Van Der Knijff, J. M., Younis, J. & De Roo, A. P. J. Lisflood: a gis-based distributed model for river basin scale water balance and flood simulation. *Int. J. Geogr. Inf. Sci.* **24:2**, 189–212 (2010).
23. Benesty, J., Chen, J., Huang, Y. & Cohen, I. Pearson correlation coefficient. In *Noise Reduction in Speech Processing*, Springer topics in signal processing, Vol. 2 (Springer, Berlin, Heidelberg, 2009).
24. Ma, L. et al. Propagation dynamics and causes of hydrological drought in response to meteorological drought at seasonal timescales. *Hydrol. Res.* **53**, 193–205 (2022).
25. Brier, G. W. Verification of forecasts expressed in terms of probability. *Mon. Weather Rev.* **78**, 1–3 (1950).
26. Laguardia, G. & Niemeier, S. On the comparison between the lisflood modelled and the ers/scat derived soil moisture estimates. *Hydrol. Earth Syst. Sci.* **12**, 1339–1351 (2008).
27. Sarailidis, G., Vasilades, L. & Loukas, A. Analysis of streamflow droughts using fixed and variable thresholds. *Hydrol. Process.* **33**, 414–431 (2019).
28. Sutanto, S. J. & Van Lanen, H. A. J. Catchment memory explains hydrological drought forecasts performance. *Sci. Rep.* **12**, 2689 (2022).
29. Clark, M. P. & Hay, L. E. Use of medium-range numerical weather prediction model output to produce forecasts of streamflow, j. hydrometeorology. *J. Hydrometeorol.* **5**, 15–32 (2004).
30. Nistor, M.-M. Groundwater vulnerability in europe under climate change. *Quat. Int.* **547**, 185–196 (2020).
31. Xanke, J. & Liesch, T. Quantification and possible causes of declining groundwater resources in the euro-mediterranean region from 2003 to 2020. *Hydrogeol. J.* **30**, 379–400 (2022).
32. Vitart, F. Evolution of ecmwf sub-seasonal forecast skill scores. *Q. J. R. Meteorol. Soc.* **140**, 1889–1899 (2014).
33. Arnal, L. et al. Skilful seasonal forecasts of streamflow over europe? *Hydrol. Earth Syst. Sci.* **22**, 2057–2072 (2018).
34. Bellprat, O. et al. Objective calibration of regional climate models: application over europe and north america. *J. Clim.* **29**, 819–838 (2016).
35. Ardilouze, C. et al. Multi-model assessment of the impact of soil moisture initialization on mid-latitude summer predictability. *Clim. Dyn.* **49**, 3959–3974 (2017).
36. Arnal, L. et al. Efas upgrade for the extended model domain. *JRC Tech. Rep. EUR29323EN, Ispra, Italy, 58pp* (2019).
37. Lorenzo-Lacruz, J., Vicente-Serrano, S. M., González-Hindalga, J. C., López-Moreno, J. I. & Cortesi, N. Hydrological drought response to meteorological drought in the iberian peninsula. *Clim. Res.* **58**, 117–131 (2013).
38. Vicente-Serrano, S. M. & López-Moreno, J. I. Hydrological response to different time scales of climatological drought: an evaluation of the standardized precipitation index in a mountainous mediterranean basin. *Hydrol. Earth Syst. Sci.* **9**, 523–533 (2005).
39. Kumar, R. et al. Multiscale evaluation of the standardized precipitation index as a groundwater drought indicator. *Hydrol. Earth Syst. Sci.* **20**, 1117–1131 (2016).
40. Haas, J. C. & Birk, S. Characterizing the spatiotemporal variability of groundwater levels of alluvial aquifers in different setting using drought indices. *Hydrol. Earth Syst. Sci.* **21**, 2421–2448 (2017).
41. Grill, G. et al. Mapping the world’s free-flowing rivers. *Nature* **569**, 215–221 (2019).
42. Canuto, N. et al. Influence of reservoir management on guadiana streamflow regime. *J. Hydrol. Reg. Stud.* **25**, 100628 (2019).
43. Pechlivanidis, I. G., Crochemore, I., Rosberg, J. & Bosshard, T. What are the key drivers controlling the quality of seasonal streamflow forecasts? *Water Resour. Res.* **56**, e2019WR026987 (2020).
44. Du, Y., Clemenzi, I. & Pechlivanidis, I. G. Hydrological regimes explain the seasonal predictability of streamflow extremes. *Environ. Res. Lett.* **18**, 094060 (2023).
45. WMO. Standardized precipitation index user guide. *WMO Rep. 1090, 24pp* <https://library.wmo.int/records/item/39629-standardized-precipitation-index-user-guide> (2012).
46. Bachmair, S., Kohn, I. & Stahl, K. Exploring the link between drought indicators and impacts. *Nat. Hazards Earth Syst. Sci.* **15**, 1381–1397 (2015).
47. Shukla, S. & Wood, A. W. Use of a standardized runoff index for characterizing hydrologic drought. *Geophys. Res. Lett.* **35**, L02405 (2008).
48. Tjeldeman, E., Stahl, K. & Tallaksen, L. M. Drought characteristics derived based on the standardized streamflow index: a large sample comparison for parametric and nonparametric methods. *Water Resour. Res.* **56**, e2019WR026315 (2020).
49. Van Lanen, H. A. J., Wanders, N., Tallaksen, L. M. & Van Loon, A. F. Hydrological drought across the world: impact of climate and physical catchment structure. *Hydrol. Earth Syst. Sci.* **17**, 1715–1732 (2013).
50. Lopez, M. G., Crochemore, L. & Pechlivanidis, I. G. Benchmarking on operational hydrological model for providing seasonal forecasts in sweden. *Hydrol. Earth Syst. Sci.* **25**, 1189–1209 (2021).
51. Trambauer, P. et al. Hydrological drought forecasting and skill assessment for the limpopo river basin, southern africa. *Hydrol. Earth Syst. Sci.* **19**, 1695–1711 (2015).
52. Johnson, S. J. et al. Seas5: the new ecmwf seasonal forecast system. *Geosci. Model Dev.* **12**, 1087–1117 (2019).
53. Hersbach, H. et al. Global reanalysis: goodbye era-interim, hello era5. *ECMWF Newsletter No. 159* <https://doi.org/10.21957/vf291hehd7> (2019).
54. Wanders, N. et al. Development and evaluation of a pan-european multimodel seasonal hydrological forecasting system. *J. Hydrometeorol.* **20**, 99–115 (2019).
55. Tourian, M. J., Schwatke, C. & Sneeuw, N. River discharge estimation at daily resolution from satellite altimetry over an entire river basin. *J. Hydrol.* **546**, 203–247 (2017).
56. Burek, P. & Smilovic, M. The use of grdc gauging stations for calibrating large-scale hydrological models. *Earth Syst. Sci. Data* **15**, 5617–5629 (2023).
57. Tapley, B. D., Bettadpur, S., Ries, J. C., Thompson, P. F. & Watkins, M. W. Grace measurements of mass variability in the earth system. *Science* **305**, 503–505 (2004).
58. Bento, V. A. et al. Persistence versus dynamical seasonal forecasts of cereal crop yields. *Sci. Rep.* **12**, 7422 (2022).
59. Lavers, D. A., Simmons, A., Vamborg, F. & Rodwell, M. J. An evaluation of era5 precipitation for climate monitoring. *Q. J. R. Meteorol. Soc.* **148**, 3152–3165 (2022).
60. Stockdale, T., Johnson, S., Ferranti, L., Balmaseda, M. & Briceag, S. Ecmwf’s new long-range forecasting system seas5. *ECMWF Newsletter No. 154* <https://doi.org/10.21957/tsb6n1> (2018).
61. Pappenberger, F., Thielen, J. & del Medico, M. The impact of weather forecast improvements on large scale hydrology: analysing a decade of forecasts of the european flood alert system. *Hydrol. Process.* **25**, 1091–1113 (2011).
62. Cloke, H., Pappenberger, F., Thielen, J. & Thiemiig, V. *Operational European flood forecasting. Environmental Modelling: Finding Simplicity in Complexity, J. Wainwright, and M. Mulligan, Eds., 2nd ed.* (John Wiley and Sons, Ltd, 2013).
63. Burek, P., van der Knijff, J. & Ntegeka, V. Lisvap evaporation pre-processor for the lisflood water balance and flood simulation model. *JRC Tech. Rep. EUR26167EN, Ispra, Italy, 42pp* (2013).
64. Sepulcre-Canto, G., Horion, S., Singleton, A., Carrao, H. & Vogt, J. Development of a combined drought indicator to detect agricultural drought in europe. *Nat. Hazards Earth Syst. Sci.* **12**, 3519–3531 (2012).
65. Yuan, X. et al. Probabilistic seasonal forecasting of african drought by dynamical models. *J. Hydrometeorol.* **14**, 1706–1720 (2013).
66. Van Hateren, T. C., Sutanto, S. J. & Van Lanen, H. A. J. Evaluating skill and robustness of seasonal meteorological and hydrological drought

- forecasts at the catchment scale - case catalonia (spain). *Environ. Int.* **133**, 105206 (2019).
67. Trambauer, P., Maskey, S., Winsemius, H., Werner, M. & Uhlenbrook, S. A review of continental scale hydrological models and their suitability for drought forecasting in (sub-saharan) africa. *Phys. Chem. Earth* **66**, 16–26 (2013).
68. Forzieri, G. et al. Ensemble projections of future streamflow droughts in europe. *Hydrol. Earth Syst. Sci.* **18**, 85–108 (2014).
69. Sutanto, S. J. & Van Lanen, H. A. J. Streamflow drought: implication of drought definitions and its application for drought forecasting. *Hydrol. Earth Syst. Sci.* **25**, 3991–4023 (2021).
70. Vicente-Serrano, S. M. et al. Accurate computation of a streamflow drought index. *J. Hydrol. Eng.* **17**, 318–332 (2012).
71. Stagge, J. H., Tallaksen, L. M., Gudmundsson, L., van Loon, A. F. & Stahl, K. Candidate distributions for climatological drought indices (spi and spei). *Int. J. Climatol.* **35**, 4027–4040 (2015).
72. Stephenson, D. B., Coelho, C. A. S., Doblus-Reyes, F. J. & Balmaseda, M. Forecast assimilation: a unified framework for the combination of multi-model weather and climate predictions. *Tellus A: Dyn. Meteorol. Oceanogr.* **57**, 253–264 (2016).

Acknowledgements

The research is supported by the CDHEU project, which is funded by the Wageningen Data Driven Discoveries in Changing Climate (D3-C2). I.G. was funded by the European Union (ERC Starting Grant, GROW- 101041110) and W.A.S. was funded by the Indonesia Endowment Fund for Education (LPDP) under the Ministry of Finance, Republic of Indonesia. The hydrometeorological outputs came from the EFAS that were downloaded from the Copernicus Data Store (CDS, see “Data availability” section). All data were processed using High Performance Computing Cluster Anunna hosted by Wageningen University and Research.

Author contributions

All authors conceived and implemented the research. Data analyses, model output analyses, and all figures have been performed by W.A.S.; S.J.S. wrote the initial version of the paper. W.A.S. and I.G. contributed to interpreting the results, discussion, and improving the paper.

Competing interests

The authors declare no competing interests.

Additional information

Supplementary information The online version contains supplementary material available at <https://doi.org/10.1038/s43247-024-01295-w>.

Correspondence and requests for materials should be addressed to Samuel Jonson Sutanto.

Peer review information *Communications Earth & Environment* thanks Jamiat Nanteza and the other, anonymous, reviewer(s) for their contribution to the peer review of this work. Primary Handling Editors: Min-Hui Lo and Aliénor Lavergne. Peer reviewer reports are available.

Reprints and permissions information is available at <http://www.nature.com/reprints>

Publisher’s note Springer Nature remains neutral with regard to jurisdictional claims in published maps and institutional affiliations.

Open Access This article is licensed under a Creative Commons Attribution 4.0 International License, which permits use, sharing, adaptation, distribution and reproduction in any medium or format, as long as you give appropriate credit to the original author(s) and the source, provide a link to the Creative Commons licence, and indicate if changes were made. The images or other third party material in this article are included in the article’s Creative Commons licence, unless indicated otherwise in a credit line to the material. If material is not included in the article’s Creative Commons licence and your intended use is not permitted by statutory regulation or exceeds the permitted use, you will need to obtain permission directly from the copyright holder. To view a copy of this licence, visit <http://creativecommons.org/licenses/by/4.0/>.

© The Author(s) 2024